Desalination and Water Treatment
www.deswater.com

doi: 10.5004/dwt.2022.28501

262 (2022) 74–88
June

Optimized electrocoagulation technology using response surface methodology to control H_2 production and treatment effect of fracturing flowback fluid treated by electrocoagulation

Zhuozhuang Liu[a,b], Wu Chen[a,b,*], Da Wu[c], Shuxia Wei[a,b], Mijia Zhu[a,b]

[a]*College of Chemical and Environmental Engineering, Yangtze University, Jingzhou, Hubei 434023, China, email: ccww91@126.com (W. Chen)*
[b]*State Key Laboratory of Control and Treatment of Petroleum and Petrochemical Pollutants (Yangtze University), Jingzhou, Hubei 434023, China*
[c]*College of Petroleum Engineering, China University of Petroleum (Huadong), Qingdao, Shandong 266580, China*

Received 2 October 2021; Accepted 7 April 2022

ABSTRACT

Fracturing flowback fluid is the most important contaminant associated with oil and gas exploration and production, which requires low-cost and sustainable technologies for treatment. This study proposed an electrocoagulation (EC) method that is time saving, highly efficient, and easy to apply to deal with this problem. A Box–Behnken design coupled with the response surface methodology (RSM) was used to construct a model of the EC process to intensively control hydrogen (H_2) production and to reduce potential safety risks while achieving high treatment efficiency. The model describes the change in the responses of decolorization rate and H_2 production in accordance with electrolysis current, plate spacing, electrolysis time, and *S*/*V*. Results show that the turbidity removal rate, decolorization rate, and H_2 production are predicted to be 87.03%, 89.14%, and 138.12 mL under the maximum H_2 production process. On the contrary, the turbidity removal rate, decolorization rate, and H_2 production are predicted to be 91.23%, 95.7%, and 7.86 mL, respectively, under minimum H_2 production conditions obtained through the model. The relative error between all the predicted and measured values is less than 2.5%. Overall, the RSM is feasible to optimize and predict the process conditions, treatment effect, and H_2 production of EC-treated fracturing flowback fluid. This optimization and prediction study can provide a reference for the efficient and safe application of EC to improve the treatment effect and control the H_2 production in the wastewater treatment process.

Keywords: Response surface methodology; Fracturing flowback fluid; Electrocoagulation; H_2 production

1. Introduction

At present, more than 80% of oil and gas fields worldwide need to be developed by using fracturing technology [1]. Hydraulic fracturing technology is an important technical means in the development and stimulation of oil and gas fields [2]. However, a large amount of fracturing flowback fluid (FFF) produces complex components after fracturing operations. The FFF has the characteristics of high stability, high chemical oxygen demand (COD), high viscosity, high total suspended solids (TSS), high total dissolved solids (TDS), high toxicity and difficult degradation [3]. The disposal methods of FFF in the domestic and international settings include reinjection into the formation, discharge or reuse after further treatment [4,5].

* Corresponding author.

Efficient use of FFF is important in the sustainable development of oil and gas fields.

At present, domestic studies on the treatment of FFF have been conducted by using flocculation, adsorption, distillation, membrane filtration, ferrocarbon microelectrolysis, oxidation, biochemical method, and combined process [6–13]. Although these methods have their own advantages, they also have problems, such as easily polluted and scaled filter membrane [14], large amount of sludge produced by flocculation method, easily passivated and blockaded filler of microelectrolysis method, and requirement of long-cycle pretreatment in the biochemical method, which should be solved [15,16]. The limited COD removal by absorption method, high organic content of the distillate by distillation [17], high running cost, long time consumption, and low efficiency by process complexity should be considered [18,19].

Electrocoagulation (EC) is an advanced technology integrating electrochemistry, coagulation, and flotation, which can remove pollutants efficiently in a short electrolysis time [20]; it has the advantages of small footprint, easy operation, easy control, high efficiency, high automation, and mild reaction conditions [21]. The EC process includes discharge, anodic oxidation, cathodic reduction, coagulation, electrophoretic migration, and adsorption [20]. During the EC process, a number of ions are generated from the anode and dissolved in the wastewater [22]. Consequently, the produced metallic hydroxides and polyhydroxides destabilize colloidal suspensions like emulsified oil, causing coagulation [23]. Destabilized colloids agglomerate into floccules and need to be removed. The electrolysis of H_2O with these impurities occurs at the anode when the treated water contains Cl^- and organic contaminants, resulting in gases, such as O_2, Cl_2, and CO_2 [24,25]. On the cathode, the electrolysis of H_2O produces H_2 [4,26]. The evolution of these gases aids in mixing and flocculation in the EC process [27,28]. The gas production mechanism and reaction of EC process are shown in Fig. 1.

EC technology has been favorably applied because of its economic effectiveness, environmental versatility, amenability of automation, and low sludge production. EC efficiently removes phosphorus [29], microplastics [30], Fluorine [31], and tannery wastewater [32], and is used for FFF treatment [33]. The EC process effectively removes the COD, chromaticity, mineralization, and other undesirable components from waste liquid, and the treated water meets the fracturing fluid preparation standard [34,35]. Fernanda et al. [34,35] presented a new process to integrate EC with granular biochar for treating FFF. The results show that the EC-biochar system achieves a 99% turbidity and TSS removal by only using 0.079 kWh/m^3, which is 70% lower than traditional DC-EC systems. The COD removal efficiency reaches 78% by using a 3D electrode/ozone system to treat the FFF from Shengli oil field in China [36]. The COD, ammonia nitrogen, and total hardness of FFF can be reduced from 1,010 mg/L; 402.5 mg/L and 234.94 mg/L to 211 mg/L, 153.23 mg/L and 230 mg/L by electrochemical method at the Changning gas field in China [37]. The COD and oil content of FFF treated by electrochemical method can be reduced from 606.4 mg/L and 153.7 mg/L to 68.5 mg/L and 9.1 mg/L [38]. Therefore, electrochemical method is effective to treat FFF.

However, most current studies focus on the effect of the electrochemical treatment of FFF and on the influence of electrochemical process conditions (such as electrode materials, current density, plate spacing, cell voltage and pH value) on the treatment effect of FFF [39] (such as removal rate of COD, chromaticity, turbidity, and oil). Few studies have been conducted on the effects of gas produced in the electrochemical treatment of waste liquid. Various side reactions easily occur during the electrochemical treatment of waste liquid, where hydrogen (H_2) is one of

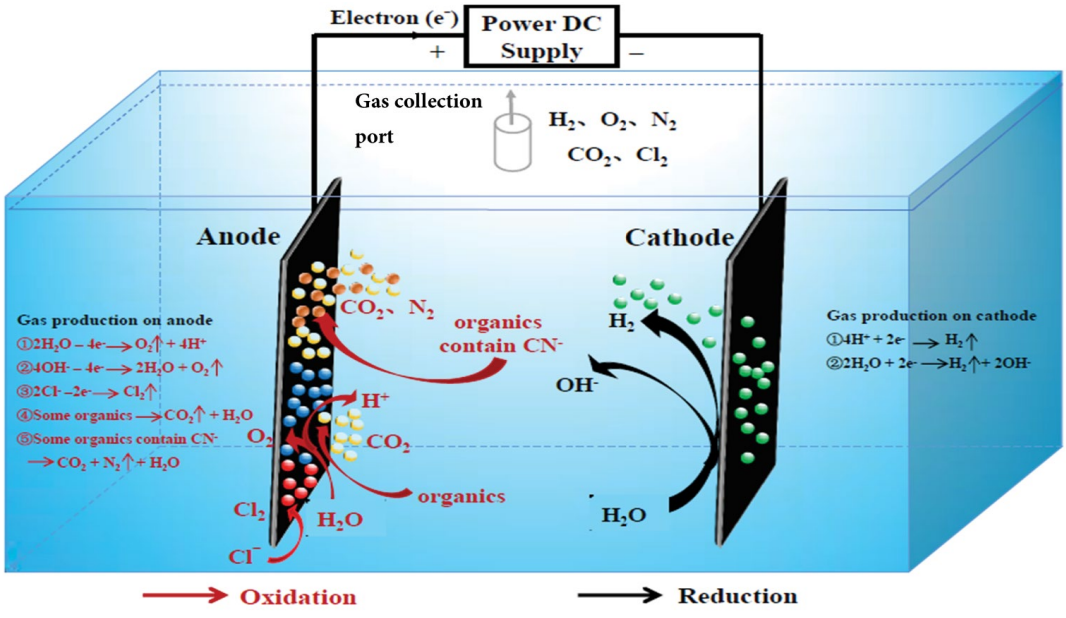

Fig. 1. Gas production mechanism and reaction of EC process.

the main byproducts of the electrochemical process [26]. For security purposes, the gas production in the electrochemical treatment of wastewater must be effectively controlled in the future application of electrochemical technology in high-risk environments, such as oil and gas fields, to improve treatment efficiency and reduce energy consumption [4,40]. Thus, investigating the factors and process conditions that influence gas production during electrochemical waste stream treatment is critical.

In this work, the amount of H_2 generated during the EC treatment of FFF was used as an index, and the response surface methodology (RSM) was used to optimize the conditions of maximum/minimum H_2 generation by the EC process to reduce the electrical consumption and H_2 generation safety risk while improving the EC treatment effect on FFF.

2. Experimental section

2.1. Experimental materials

The FFF samples used in our experiment are obtained from the Fuling Shale Gas Field station 44, Jianghan Oilfield, Sinopec, Fuling District, Chongqing, China. Table 1 shows its characteristics and analytical methods/instrument.

2.2. Experimental apparatus

Fig. 2a shows a diagram of the EC device. The experimental work was conducted by using a set of devices that can continuously monitor the effect of the EC treatment of waste liquid and gas production in the electrolytic process. The devices used were as follows: (1) The power supply was WYK–60V30A programmable DC power supply type XR (input voltage = AC220 V ± 10%, 50 ± 1 Hz; output voltage = 0–60 V; output current = 0–30 Å) (Shanghai Yize Electric Co., Ltd.). (2) An electrolytic tank was used to collect gas from waste liquid through the EC treatment (total volume = 3,538.08 mL). The main components of the electrolytic tank included electrolysis, buffer, and overflow rooms. The dimensions of the electrolysis, buffer, and overflow rooms were 120 mm × 144 mm × 105 mm (total volume = 1,814.4 mL), 20 mm × 144 mm × 135 mm (total volume = 388.8 mL), and 30 mm × 144 mm × 105 mm (total volume = 583.2 mL), respectively. The tank was produced by Feihong Plexiglass Products Company in Jianghan District, Wuhan, China. (3) An electrode combination made up of a plate-like aluminum anode and a plate-like aluminum cathode was placed in parallel and vertically with a separation distance of 2.0 cm to 10.0 cm. The standard dimensions (length × width × thickness) were 100 mm × 90 mm × 3 mm. The electrode was produced by Baoji Longsheng Nonferrous Pioneer Metals Company, China. (4) The gas flow meter and accumulation meter type were MFM610–RS232 (range = 0–300 mL/min, Suzhou AituoliElectronic Equipment Co., Ltd). (5) A GT-2000 pumping mixed gas analyzer (accuracy = 1%–3%, Shenzhen Kolno Electronic Technology Co., Ltd.) was used.

2.3. Experimental method

2.3.1. Method of EC experiment and H_2 production measurement

At room temperature, the FFF (800 mL) collected from the Fuling oil and gas field was added to an electrolytic tank capable of collecting gas generated by the EC treatment of waste liquid. The electrode combinations for electrochemical experiments were selected as follows: plate-like aluminum anode and plate-like aluminum cathode. The electrode in the EC reactor was connected in a monopolar arrangement. The FFF was electrochemically treated under different conditions (electrolytic conditions: I = 0.5–2.5 A, t = 20–70 min, and d = 2.0–10.0 cm, where I is the electrolysis current; t is the electrolysis time; d is the distance between the cathode and the anode). When the DC power was switched on, the gas generated in the treatment process entered the dehumidifier through the duct to remove moisture and then entered the gas accumulation meter to record the total amount of gas produced. The generated gas entered the pump-type mixed gas analyzer for composition and content analyses, automatically recording and storing each component data. The EC treatment and gas production monitoring processes are shown in Fig. 2b.

2.3.2. Determination methods of color and turbidity

After each EC treatment, the treated FFF samples were collected to determine the color and turbidity. Color was determined by spectrophotometry with a 751-GW UV/vis spectrophotometer (Inesa Analytical Instrument Co., Ltd., Shanghai, China) [4]. The maximum absorption wavelength

Table 1
Characteristics of the FFF of Fuling

Parameters	Values	Analytical instruments	Methods
pH	8.0	pH meter (PB-10, Sartorius, Germany)	[41]
Color	499.53	Spectrophotometry[a]	[42]
TOC (mg/L)	350.73	Total organic carbon analyser (Vario TOC cube, Elementar, Germany)	[43]
Salinity (mg/L)	33,227.34	RFIC (ICS-2000, Dionex, USA)	[44]
Oil (mg/L)	137.11	Infrared oil spectrometer (JC-OIL-6, Juchuang, China)	[45]
COD (mg/L)	1,620.0	/	[46]
Turbidity (NTU)	246.0	Digital turbidimeter (AQ2010, Thermo, USA)	[47]

TOC: total organic carbon; COD: chemical oxygen demand; SS: suspended solids.

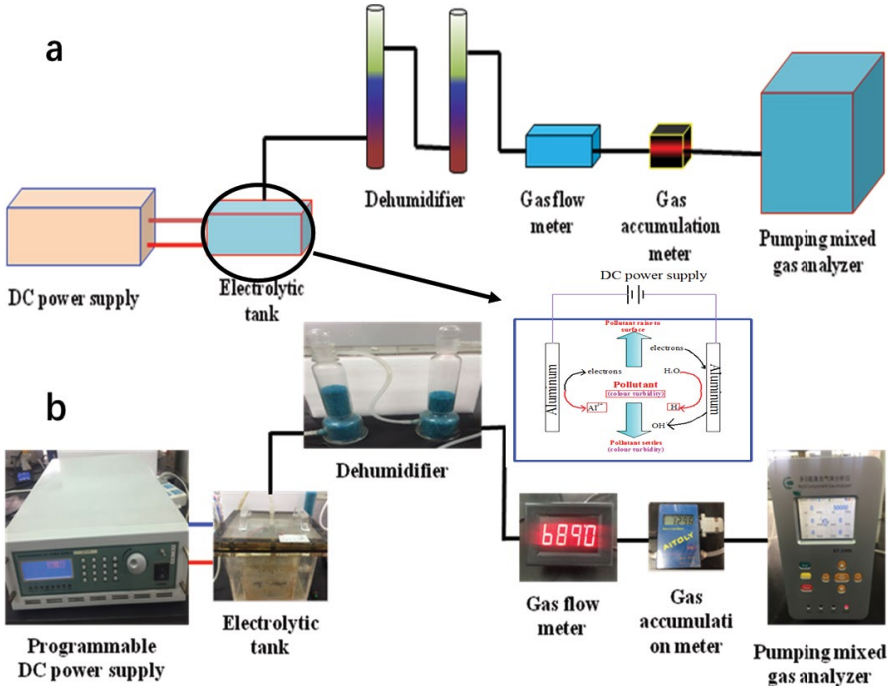

Fig. 2. (a,b) Schematic of the electrochemical device.

Table 2
Table of experimental factors

Original factors (x)	Level		
	−1	0	1
x_1 (electrolysis current) (Å)	0.5	1.0	1.5
x_2 (plate spacing) (cm)	4.0	6.0	8.0
x_3 (electrolysis time) (min)	20.0	30.0	40.0
x_4 (S/V) (cm²/mL)	0.10	0.11	0.12

at 339 nm was obtained by determining the color. Standard solution samples were prepared from a commercial concentrated platinum cobalt color solution. The samples were used for instrument calibration and for the development of a standard curve of color and absorbance. The R^2 value associated with this curve was 0.9999. Decolorization rate was calculated by using the following equation: $R\% = [(A_0 - A)/A_0] \times 100$, where A_0 and A are the initial and final absorbance of FFF before and after treatment, respectively. Turbidity was determined by using a turbidity meter (Orion AQ2010, Thermo Electron Corporation). Turbidity removal rate was calculated with the following equation: $R\% = [(T_0 - T)/T_0] \times 100$, where T_0 and T are the initial and final turbidity of FFF before and after treatment, respectively.

2.3.3. Calculated method of anode consumption rate

After each EC treatment, the aluminum anode was removed from the electrolytic tank, and its quality was weighed after cleaning and drying. The aluminum anode plate consumption rate is calculated as follows:

$$C\% = \frac{(M_0 - M)}{(S \times t)} \times 100 \quad (1)$$

where M_0 (mg) and M (mg) are the initial and final anode aluminum plate qualities, respectively; S (m²) is the area of the anode aluminum plate in the solution; t (h) is the EC reaction time.

2.4. RSM experimental design

RSM is a comprehensive calculation model based on statistics, which is used to explain the effect of multiple specific variables on a system or structure, and is the conversion relationship between input (variables) and output (response) of the system or structure [48,49]. RSM is considered an effective means in experiment design to evaluate the relative importance of variables and their interactions and to build a model for process optimization and effect prediction for reducing the number of experimental trials [50].

In accordance with the principle of RSM, the Box–Behnken design (BBD) was used to create a set of designed experiments on Design Expert 8.0.6 software [51]. This experimental design was performed as a BBD composed of 29 experiments. The empirical model represented by a second-order polynomial regression used to describe the system behavior was calculated by using Eq. (2).

$$Y = \beta_0 + \sum_{i=1}^{k} \beta_i x_i + \sum_{i=1}^{j=1} \sum_{j=1}^{k} \beta_{ij} x_i x_j + \sum_{j=1}^{k} \beta_{ii} x_i^2 + \varepsilon \quad (2)$$

where Y represents the response values, β_0, $\beta_{1\ldots4}$, $\beta_{11\ldots44}$, and $\beta_{12,13,23,24}$ are the main (linear), interaction, and quadratic

effect coefficients, x_1, x_2, x_3, x_4 are the independent variables, and ε is the error.

The BBD for four factors, such as electrolysis current (x_1), plate spacing (x_2), electrolysis time (x_3), and the ratio of the effective cathode surface to the volume of FFF (Abbreviation: *S*/*V*) (x_4), and decolorization rate (Y_1), turbidity removal rate (Y_2), and H_2 production (Y_3) are used as the response values to design the experimental scheme. The purpose of this experimental design is to analyze the interactive effect of the four factors (x_1, x_2, x_3, and x_4) and find the optimum operational condition in terms of the optimization objectives of response values (Y_1, Y_2, and Y_3) by RSM–BBD.

3. Results and discussion

3.1. Effects of the EC operating parameters

In this study, aluminum electrode plates were used to treat FFF because the flocs produced by the Al electrode have fast speed, high decolorization rate, and strong adsorption capacity, and the H_2 production of Al electrode plates is under the same conditions, which is convenient for the study of H_2 production [51].

When aluminum was used as electrode materials, the reactions were as follows:

At the anode

$$Al \rightarrow Al^{3+} + 3e \quad (3)$$

At the cathode

$$3H_2O + 3e \rightarrow \frac{3}{2}H_2(g) + 3OH^- \quad (4)$$

In the solution

$$Al^{3+}(aq) + 3H_2O \rightarrow Al(OH)_3 + 3H^+(aq) \quad (5)$$

This experiment mainly aimed to study the influence of electrolysis time, current, electrode spacing, and *S*/*V* on H_2 production, decolorization rate, turbidity removal rate, and anode consumption to provide a basis for the selection of the appropriate level of the four factors of BBD.

3.1.1. Effect of electrolysis current

Electrolysis current is extremely important in EC because it is the key operational parameter that can be controlled directly and it directly determines coagulant dosage and gas generation rates. Thus, the experiment of FFF treated by EC was conducted under the condition of *S*/*V* = 0.11 cm²/mL, *d* = 4.0 cm, and *t* = 30.0 min. The treatment effect of EC, the consumption rate of anode plate, and the H_2 production were measured under different electrolytic currents. The results are shown in Fig. 3a and b.

With the increase in electrolysis current, the decolorization and turbidity removal rates decreased, whereas the H_2 production and anode plate consumption rates increased linearly (Fig. 3a and b). The increase in electrolysis current produced excessive Al^{3+} [53,54], which reversed the colloid's surface charge, formed colloidal repelling, destroyed the floc, and decreased the flocculation ability, thereby increasing the turbidity and color of the waste liquid [55]. On the contrary, the electrolytic bubble size decreases with the increase in current density. However, the nucleated small bubbles coalesced, created coarse bubbles, and reduced the treatment efficiency when the applied current density surpassed a threshold. Therefore, an optimum current density produces the finest bubbles, and the applied current affects the energy consumption and the treatment system [56]. When the electrolysis current was 0.5 A, H_2 production was minimal, plate consumption was low, and the decolorization and turbidity removal rates were 95.92% and 88.21%, respectively. Thus, 0.5 A was chosen as the follow-up electrolysis current.

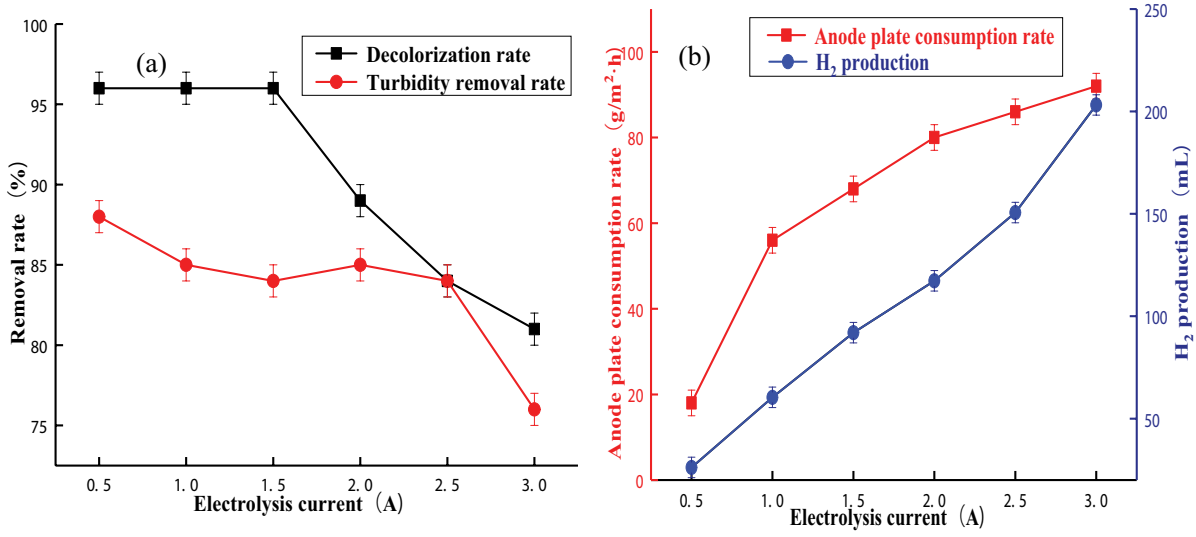

Fig. 3. Effect of electrolysis current on (a) decolorization rate and turbidity removal rate and (b) anode plate consumption rate and H_2 production.

3.1.2. Effect of plate spacing

The electrode spacing is a control parameter that affects the reactor size, reaction, and energy consumption; it also has an important influence on the overall treatment cost [27]. Therefore, the experiment on FFF treated by EC was conducted under the condition of S/V = 0.11 cm^2/mL, t = 30.0 min, and I = 0.5 A, and the treatment effects, anode plate consumption rate, and H_2 production were measured under different plate spacing values. The results are shown in Fig. 4a and b.

A narrow space between the plates was unconducive to the solution flowing between the two plates (Fig. 4a and b). The H_2 bubbles generated by electrolysis cause the water sample to fluctuate; thus, the pollutants become uneven and affect the stability of the treatment effect. This result is consistent with the reported results in the literature [57]. When the distance between the plates is considerably large, the resistance between the two poles increases, and the dissolved Al^{3+} is minimal. Thus, the flocculation effect is unremarkable with the minimal Al^{3+} hydrolyzed polymer formed [58]. Excessively large plate spacing may increase the activation energy of the electrolysis reaction, decrease the electrode reaction speed, prolong the electrolysis time, increase the concentration polarization, and reduce the H_2 production and electrolysis efficiency. If the plate spacing is extremely short, then the short circuit and the flocs are easily blocked between plates. Therefore, extremely long or short plate spacing is unconducive to improving the EC efficiency and reducing the energy consumption [59]. When the distance between the plates was 8.0 cm, the anode plate consumption rate was low, H_2 production was small, and the decolorization and turbidity removal rates were more than 94%. Thus, the plate spacing of 8.0 cm was suitable in this experiment.

3.1.3. Effect of electrolysis time

In accordance with Faraday's law, electrolysis time affects the amount of anode dissolved (metal ions, for example, Al^{3+}) when the current is constant. Thus, the amount of coagulant, the amount of gas (H_2 and O_2) released by electrolysis, and the efficiency of electrolytic treatment are affected. Therefore, the experiment on FFF treated by EC was conducted under the condition of S/V = 0.11 cm^2/mL, d = 8.0 cm, and I = 0.5 A. The treatment effect of EC, the consumption rate of anode plate, and the H_2 production were measured under different electrolytic periods. The results are shown in Fig. 5a and b.

The turbidity removal and decolorization rates, H_2 production, and anode plate consumption rate increased with the increase in electrolysis time (Fig. 5a and b). With the increase in electrolysis time, the anode plate consumption rate increased, the Al^{3+} produced by electrolysis rapidly produced in the form of hydrated ion $Al(H_2O)_6^{3+}$ in water, formed a series of mononuclear complexes, such as $Al(H_2O)_5OH^{2+}$, $Al(H_2O)_4(OH)_2^+$, and $Al(H_2O)_3(OH)_3$, and transformed into an amorphous $[Al(OH)_3]_n$ flocculant [60,61]. H_2 continuously evolved from the cathode plate, the concentration polarization of the cathode was effectively avoided under the combined action of Al^{3+} and H_2, and the decolorization and turbidity removal rates continuously increased. If the electrolysis time is extremely long, then the electrolysis produced excessive Al^{3+} to diffuse and flocculate. Thus, the treatment effect decreased, and the energy consumption increased. Given the treatment effect and plate consumption, the electrolysis time was 30.0 min.

3.1.4. Effect of S/V

When I, d, and t are fixed, S/V affects the amount of anode dissolved, the amount of gas (H_2 and O_2) released

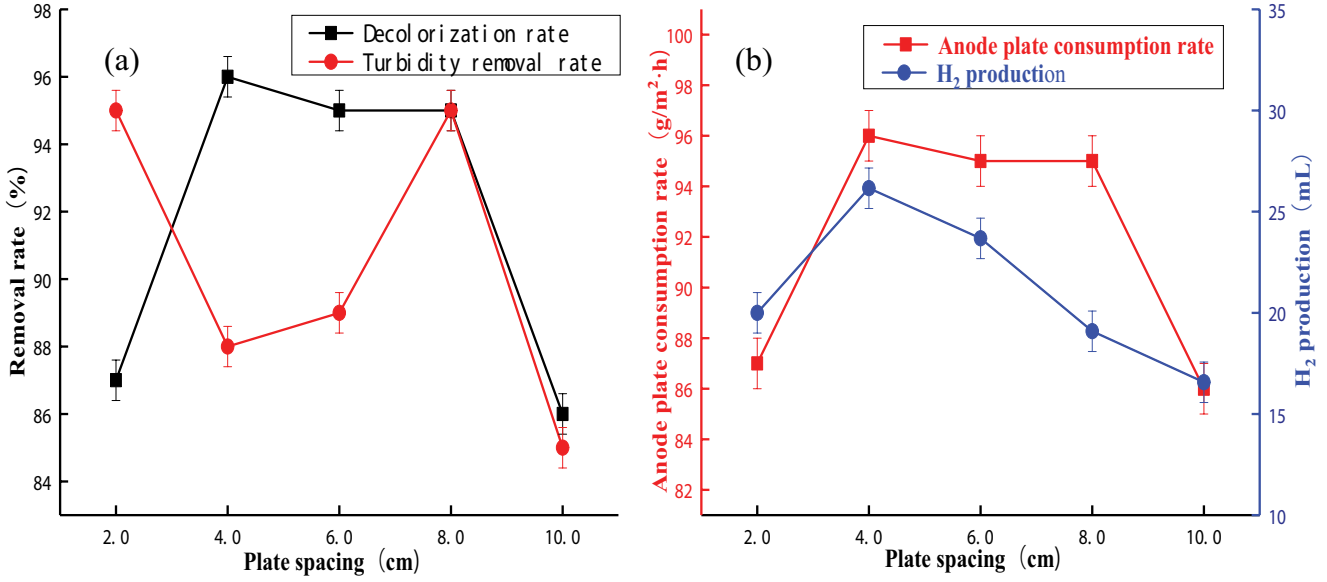

Fig. 4. Effect of plate spacing on (a) decolorization rate and turbidity removal rate and (b) anode plate consumption rate and H_2 production.

by electrolysis, and the efficiency of electrolytic treatment. The experiment on FFF treated by EC was conducted under the conditions of I = 0.5 A, d = 8.0 cm, and t = 30.0 min. The effects of the EC treatment of FFF, anode plate consumption rate, and H_2 production were measured under different S/V values. The results are shown in Fig. 6a and b.

With the increase in S/V, the anode plate consumption rate and H_2 production decreased continuously (Fig. 6a and b). In the initial electrolysis stage, the S/V was probably small, H_2 production was high, and the disturbance effect was substantial [62], exacerbating the treatment effect. Under a stable current, the S/V increased, the effective area of electrodes increased, the current density decreased, and the production of Al^{3+} from Al anode dissolution decreased. Thus, the flocculation treatment effect and H_2 production from the Al cathode decreased. The S/V was selected as 0.11 cm^2/mL to ensure a certain treatment effect.

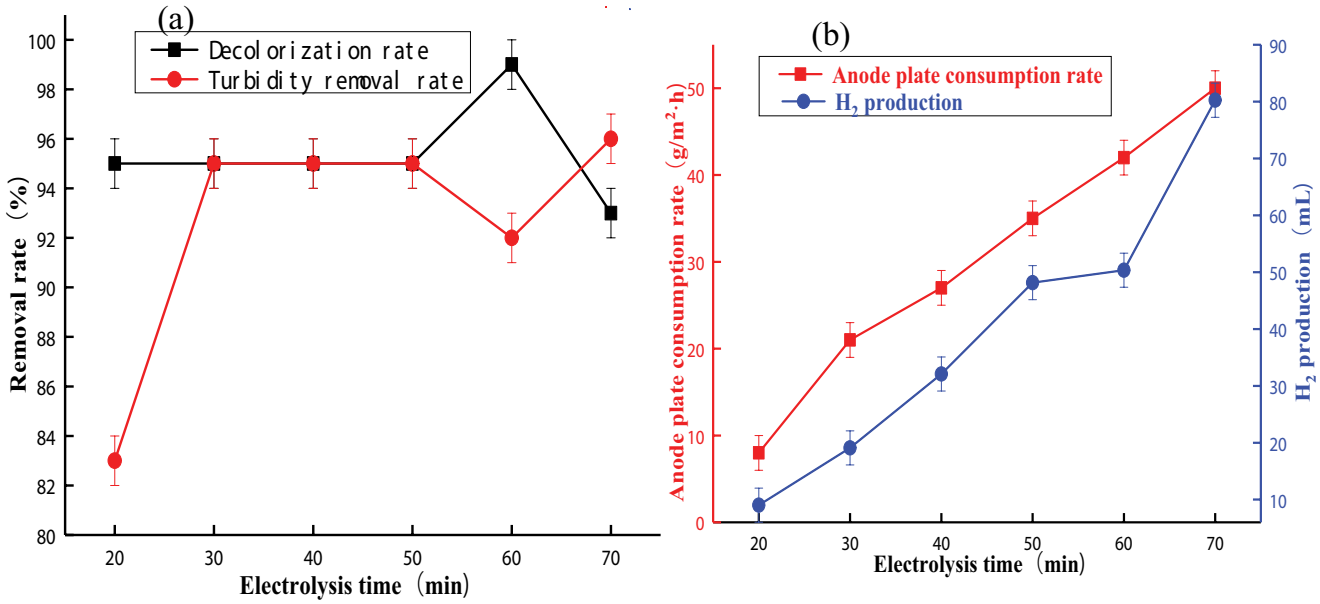

Fig. 5. Effect of electrolysis time on (a) decolorization rate and turbidity removal rate and (b) anode plate consumption rate and H_2 production.

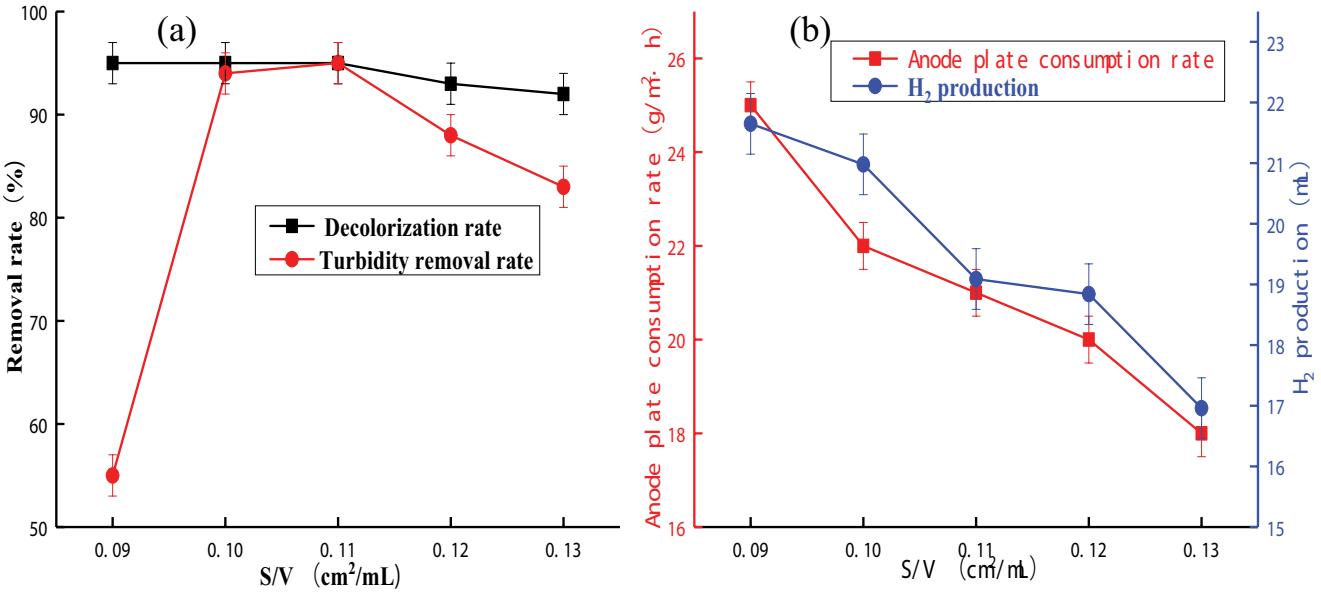

Fig. 6. Effect of S/V on (a) decolorization rate and turbidity removal rate and (b) anode plate consumption rate and H_2 production.

Table 3
BBD with four factors and its measured and predicted values

Trial.	Current (x_1)(Å)	Spacing (x_2)(cm)	Time (x_3) (min)	S/V (x_4) (cm^2/mL)	Decolorization rate (Y_1)(%)		Turbidity removal rate (Y_2)(%)		H_2 production (Y_3)(mL)	
					Experimental	Predicted	Experimental	Predicted	Experimental	Predicted
1	0.5	4.0	30.0	0.11	95.92	97.21	88.21	86.32	26.16	26.54
2	1.5	4.0	30.0	0.11	96.15	96.07	83.74	81.72	91.96	91.18
3	0.5	8.0	30.0	0.11	94.69	96.22	95.12	90.05	19.09	17.68
4	1.5	8.0	30.0	0.11	92.08	92.24	84.96	85.44	102.30	99.73
5	1.0	6.0	20.0	0.10	85.92	88.25	82.93	84.29	24.48	34.46
6	1.0	6.0	40.0	0.10	45.23	59.91	83.33	80.63	79.10	91.10
7	1.0	6.0	20.0	0.12	92.08	78.85	95.93	91.13	36.72	24.74
8	1.0	6.0	40.0	0.12	94.23	93.35	82.11	87.47	94.79	84.82
9	0.5	6.0	30.0	0.10	85.08	82.63	84.15	84.77	22.08	16.32
10	1.5	6.0	30.0	0.10	78.85	77.41	78.05	80.16	119.21	109.24
11	0.5	6.0	30.0	0.12	91.00	92.00	80.08	91.61	20.79	27.89
12	1.5	6.0	30.0	0.12	90.08	92.09	89.02	87.00	78.79	81.67
13	1.0	4.0	20.0	0.11	90.00	90.87	82.93	85.85	36.39	27.54
14	1.0	8.0	20.0	0.11	91.92	95.04	84.96	89.58	28.83	31.66
15	1.0	4.0	40.0	0.11	94.08	90.52	89.02	82.19	90.54	90.18
16	1.0	8.0	40.0	0.11	82.85	81.54	78.05	85.92	74.43	85.75
17	0.5	6.0	20.0	0.11	88.92	92.20	87.80	90.02	8.53	10.96
18	1.5	6.0	20.0	0.11	91.08	94.71	86.18	85.41	40.45	48.24
19	0.5	6.0	40.0	0.11	95.00	90.35	90.24	86.36	41.33	33.25
20	1.5	6.0	40.0	0.11	87.00	82.71	76.01	81.75	145.38	142.67
21	1.0	4.0	30.0	0.10	88.08	82.77	75.20	80.60	70.32	69.11
22	1.0	8.0	30.0	0.10	84.08	76.28	82.93	84.33	67.56	56.46
23	1.0	4.0	30.0	0.12	83.92	90.71	82.52	87.44	40.71	48.61
24	1.0	8.0	30.0	0.12	88.08	92.38	97.97	91.17	62.94	60.95
25	1.0	6.0	30.0	0.11	94.00	94.00	89.84	85.88	56.36	58.78
26	1.0	6.0	30.0	0.11	94.00	94.00	89.84	85.88	56.36	58.78
27	1.0	6.0	30.0	0.11	94.00	94.00	89.84	85.88	56.36	58.78
28	1.0	6.0	30.0	0.11	94.00	94.00	89.84	85.88	56.36	58.78
29	1.0	6.0	30.0	0.11	94.00	94.00	89.84	85.88	56.36	58.78

3.2. RSM optimization

When I = 0.5 A, d = 8.0 cm, t = 30.0 min, and S/V = 0.11 cm²/mL, the decolorization and turbidity removal rates were above 94% in the single factor experiment.

The results of single factor experiment showed that the decolorization and turbidity removal rates are above 94% when I = 0.5 A, d = 8.0 cm, t = 30.0 min, and S/V = 0.11 cm²/mL. The levels of influencing factors x_1, x_2, x_3, and x_4 were determined on the basis of these results, combined with the RSM experimental design, as shown in Table 2.

In accordance with the RSM design principles, 29 groups of experiments were conducted at the factor level shown in Table 2. The test results are shown in Table 3.

Table 3 summarizes the results of the experiments for the parameters affecting the evaluation process and the prediction values obtained from the model. The results obtained from the proposed model are slightly the same with the actual results obtained [63]. The regression equation was obtained by using Design Expert to conduct multivariate regression fitting analysis on the experimental data presented in Table 3.

$$\begin{aligned} Y_1 = {} & -672.48625 - 20.01x_1 - 7.58458x_2 - 7.64808x_3 \\ & + 16{,}166.83333x_4 - 0.71x_1x_2 - 0.508x_1x_3 + 265.5x_1x_4 \\ & - 0.16438x_2x_3 + 102x_2x_4 + 107.1x_3x_4 + 3.87167x_1^2 \\ & + 0.11698x_2^2 - 0.049746x_3^2 - 89{,}345.83333x_4^2 \end{aligned} \quad (6)$$

$$Y_2 = +52.7708 - 4.60667x_1 + 0.93208x_2 - 0.18308x_3 + 342x_4 \quad (7)$$

$$\begin{aligned} Y_3 = {} & +76.61707 + 154.25667x_1 - 35.54625x_2 - 0.99592x_3 \\ & - 576.58333x_4 + 4.3525x_1x_2 + 3.6065x_1x_3 - 1{,}956.5x_1x_4 \\ & - 0.10688x_2x_3 + 312.375x_2x_4 + 8.625x_3x_4 \end{aligned} \quad (8)$$

The regression equation indicated that the effect of each factor on the decolorization rate, turbidity removal rate, and H_2 production was an interactive linear relationship. A variance analysis of the model was performed to verify the sufficiency and significance of the response surface model in simulating the experimental results. The results of variance analysis of the regression model are shown in Tables 4–6.

For the decolorization rate (Table 4), the F-value and P-value were 2.84 and 0.0302 (less than 0.05), respectively, implying that the model was significant and suitable to demonstrate the relationship between independent variables and response. The P-values less than 0.05 indicated that the model terms x_4, x_1x_3, x_3x_4, and x_4^2 are significant, as described in Table 4. For the in-group rating, the F-value and P-value of the turbidity removal rate (Table 5) and H_2 production (Table 6) show that the effect of the model is significant, and the method is reliable. The P-values less than 0.05 indicated that the model term x_4 is significant, as described in Table 5. The P-values less than 0.05 indicated that the model terms x_1, x_3, x_1x_3, and x_1x_4 are significant, as described in Table 6.

Figs. 7–9 show the standardized Pareto charts for decolorization rate, turbidity removal rate, and H_2 production. These Pareto charts display a frequency histogram where the length of each bar is proportional to the estimated effect and interaction of the factors on the response [64]. In the Pareto charts, the cross line indicates the significance of each parameter, and the strip across the reference line is statistically significant.

In Fig. 7, the interaction between electrolytic time and S/V influenced significantly the decolorization rate. Table 4 shows that the F-values of the electrolysis current, plate spacing, electrolysis time, and S/V are 0.42, 0.37, 3.07, and 9.26, respectively. Thus, the order of significant influence on the decolorization rate is S/V. In Fig. 8, only S/V influenced significantly the turbidity removal rate. In Fig. 9, electrolysis current, electrolysis time, the interaction between electrolytic time and electrolysis current, and the interaction between electrolysis current and S/V influenced significantly the H_2 production. Table 6 illustrates that the order of significant influence on H_2 production is electrolysis current > electrolysis time. The results of the variance analyses showed that the regression equation has a guiding effect on the experiment throughout the experimental interval.

The 3D response surface plots of the interaction among various factors were drawn to intuitively reflect the influences of electrolysis current, plate spacing, electrolysis time, and S/V on the turbidity removal decolorization rates and H_2 production (Figs. 10–12). These representations were extremely useful for evaluating the relationship between independent and dependent variables.

As shown in Fig. 10, the graphs represent the effects of electrolysis current, plate spacing, electrolysis time, and S/V on decolorization by varying two parameters while the others are kept constant in their zero level. The interaction between electrolysis time and S/V at ultrasonic time of electrolysis current (1.0 A) and plate spacing (6.0 cm) is illustrated in Fig. 10a6. The elliptical contour lines indicated that the interactions are large and important, thereby verifying the term x_3x_4 in Eq. (6) and Table 5. As illustrated by the gradient in the surface plot, the electrolysis time and S/V were dominant in the interactive effect of EC on the decolorization.

Figs. 11 and 12 represent the effects of electrolysis current, plate spacing, electrolysis time, and S/V on the turbidity removal rates and H_2 production by varying two parameters while the others are kept constant in their zero level. In Fig. 11b3, for a constant initial plate spacing and electrolysis time (with 6.0 cm and 30 min), decreased S/V and increased electrolysis current led to significantly improved turbidity removal rates (from 80.08% to 84.15%). In Fig. 12c3, for a constant initial plate spacing, S/V, and electrolysis time (with 6.0 cm, 0.11 cm²/mL, and 40 min), increased electrolysis current led to significantly improved H_2 production (from 41.33 to 145.38 mL). The elliptical contour lines indicated that the interactions are large and important, thereby verifying Eqs. (7) and (8) and Tables 6 and 7. As illustrated by the gradient in the surface plot, the electrolysis current and S/V were dominant in the interactive effect of EC on turbidity removal rates, and electrolysis current was dominant in the interactive effect of EC on H_2 production.

Table 4
Variance analysis of the decolorization rate regression model

Source	Sum of squares	df	Mean square	*F*-value	*P*-value	Significance
Model	1,863.80	14	133.13	2.84	0.0302	significant
x_1	19.69	1	19.69	0.42	0.5274	not significant
x_2	17.40	1	17.40	0.37	0.5521	not significant
x_3	143.73	1	143.73	3.07	0.1018	not significant
x_4	433.80	1	433.80	9.26	0.0088	significant
x_1x_2	2.02	1	2.02	0.043	0.8387	not significant
x_1x_3	25.81	1	25.81	0.55	0.4704	significant
x_1x_4	7.05	1	7.05	0.15	0.7040	not significant
x_2x_3	43.23	1	43.23	0.92	0.3532	not significant
x_2x_4	16.65	1	16.65	0.36	0.5607	not significant
x_3x_4	458.82	1	458.82	9.79	0.0074	significant
x_1^2	6.08	1	6.08	0.13	0.7242	not significant
x_2^2	1.42	1	1.42	0.030	0.8643	not significant
x_3^2	160.52	1	160.52	3.42	0.0854	not significant
x_4^2	517.80	1	517.80	11.05	0.0050	significant
Residual	656.21	14	46.87			
Lack of fit	656.21	10	65.62	1.40	0.2565	not significant
Pure error	187.52	4	46.88			
Cor. total	2,520.00	28				

Table 5
Variance analysis of the turbidity removal rate regression model

Source	Sum of squares	df	Mean square	*F*-value	*P*-value	Significance
Model	285.95	4	71.49	2.82	0.0474	significant
x_1	63.66	1	63.66	2.51	0.1260	not significant
x_2	41.70	1	41.70	1.65	0.2118	not significant
x_3	40.22	1	40.22	1.59	0.2198	not significant
x_4	140.36	1	140.36	5.54	0.0271	significant
Residual	608.06	24	25.34			
Lack of fit	608.06	20	30.40	1.20	0.4157	not significant
Pure error	101.40	4	25.35			
Cor. total	894.00	28				

3.3. Optimization of process parameters and verification of the model

The process parameters were optimized by using the numerical optimization tool Design Expert 8.0.6. An experiment was conducted to verify the optimum results obtained from model prediction. In the optimization process, different weights were assigned to the response values, and the weights of decolorization rate (Y_1), turbidity removal rate (Y_2), and H_2 production (Y_3) were + + +, + + +, and + + + + +, respectively, to consider the control of H_2 production and treatment effect. The optimization objective is that Y_1 and Y_2 should reach the maximum value regardless of whether Y_3 is the maximum or minimum. The results are shown in Table 7.

As shown in Table 7, the maximum H_2 production process parameters were I = 1.5 A, d = 8.0 cm, t = 40.0 min, and S/V = 0.12 cm²/mL. The predicted maximum H_2 production was 138.12 mL, and the turbidity removal and the decolorization rates were 87.03% and 89.14%, respectively. Under this condition, the measured H_2 production, turbidity removal rate, and decolorization rate were 140.38 mL, 85.96%, and 87%, respectively, and the relative errors were 1.61%, 1.24%, and 2.46%. The results showed that the minimum H_2 production process parameters were I = 0.5 A, d = 8.0 cm, t = 20.0 min, and S/V = 0.11 cm²/mL, and the predicted minimum H_2 production was 7.86 mL. The turbidity removal rate and the decolorization rate were 91.23% and 95.7%, respectively. Under this condition, the measured H_2 production, turbidity removal rate, and decolorization rate were 7.95 mL, 89.52%, and 95.23%, respectively, and the relative errors were 1.13%, 1.91%, and 0.49%, respectively. These results indicate that the treatment effect of EC with maximum H_2 production is

Table 6
Variance analysis of the H_2 production regression model

Source	Sum of squares	df	Mean square	*F*-value	*P*-value	Significance
Model	28,488.43	10	2,848.84	40.66	0.0001	significant
x_1	16,141.40	1	16,141.40	230.35	0.0001	significant
x_2	0.072	1	0.072	0.001029	0.9748	not significant
x_3	10,218.25	1	10,218.25	145.82	0.0001	significant
x_4	192.08	1	192.08	2.74	0.1151	not significant
x_1x_2	75.78	1	75.78	1.08	0.3122	not significant
x_1x_3	1,300.68	1	1,300.68	18.56	0.0004	significant
x_1x_4	382.79	1	382.79	5.46	0.0312	significant
x_2x_3	18.28	1	18.28	0.26	0.6158	not significant
x_2x_4	156.13	1	156.13	2.23	0.1528	not significant
x_3x_4	2.98	1	2.98	0.042	0.8391	not significant
Residual	1,261.32	18	70.07			
Lack of fit	1,261.32	14	90.09	1.29	0.3201	not significant
Pure error	280.24	4	70.06			
Cor. total	29,749.76	28				

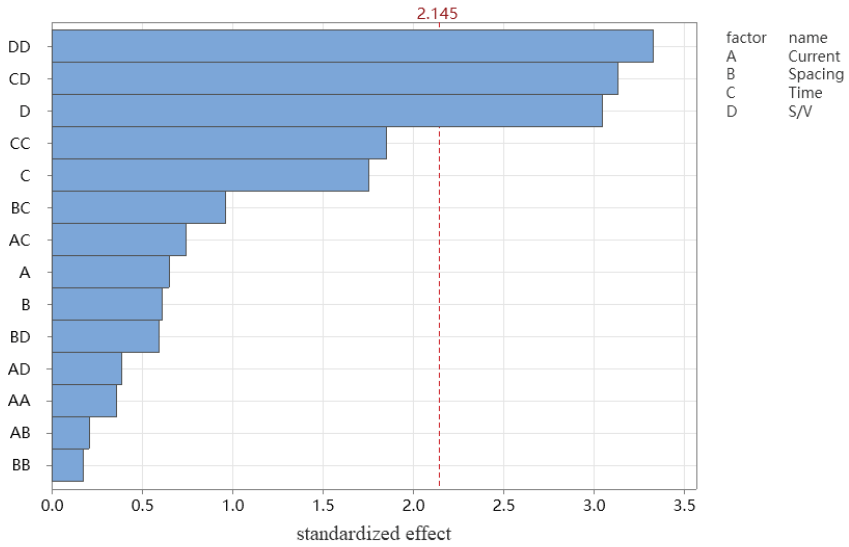

Fig. 7. Standardized Pareto chart for decolorization rate.

Table 7
RSM predicted and actual values

Minimum/Maximum H_2 production process parameters	Indicators	RSM predictive values	Actual values	Relative error (%)
I = 0.5 A; d = 8.0 cm;	Decolorization rate (%)	95.70	95.23	0.49
t = 20.0 min;	Turbidity removal rate (%)	91.23	89.52	1.91
S/V = 0.11 cm²/mL	H_2 production (mL)	7.86	7.95	–1.13
I = 1.5 A; d = 8.0 cm;	Decolorization rate (%)	89.14	87.00	2.46
t = 40.0 min;	Turbidity removal rate (%)	87.03	85.96	1.24
S/V = 0.12 cm²/mL	H_2 production (mL)	138.12	140.38	1.61

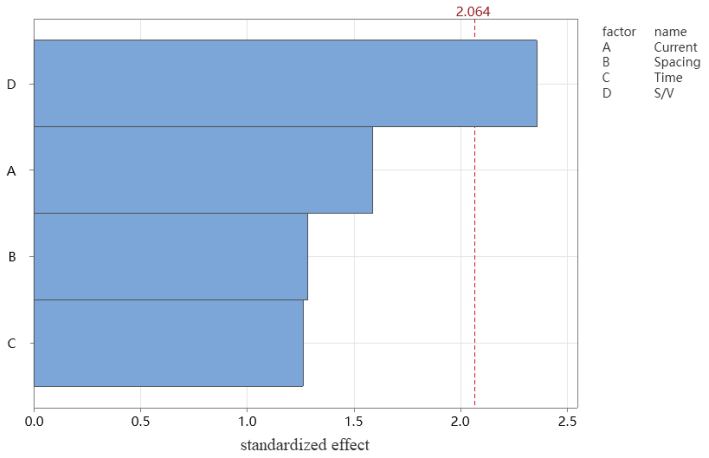

Fig. 8. Standardized Pareto chart for turbidity removal rate.

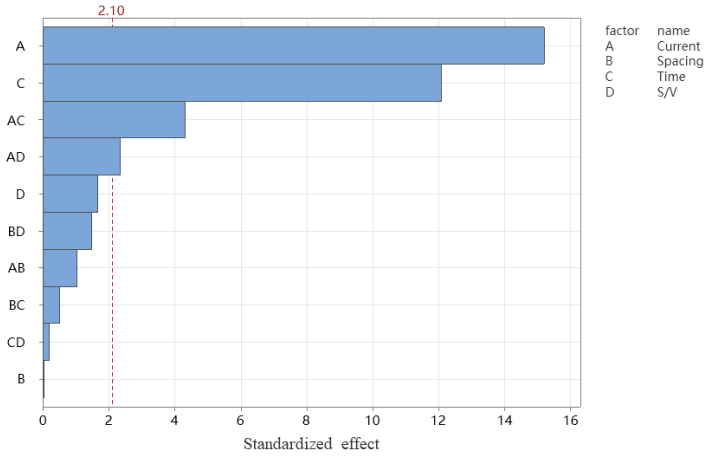

Fig. 9. Standardized Pareto chart for H_2 production.

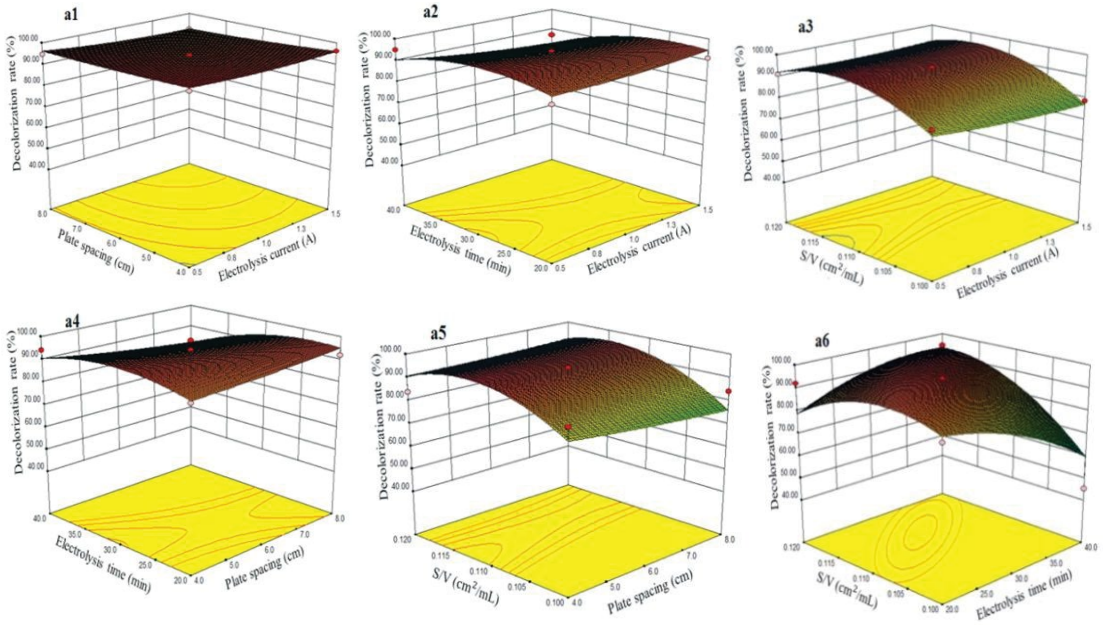

Fig. 10. Effects of electrolysis current, plate spacing, electrolysis time, and *S/V* on decolorization.

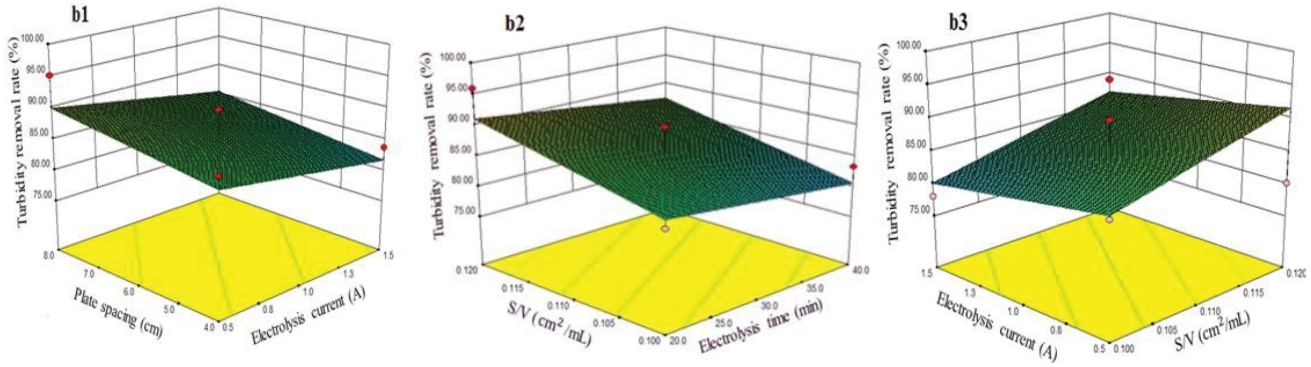

Fig. 11. Effects of electrolysis current, plate spacing, electrolysis time, and *S*/*V* on turbidity removal rates.

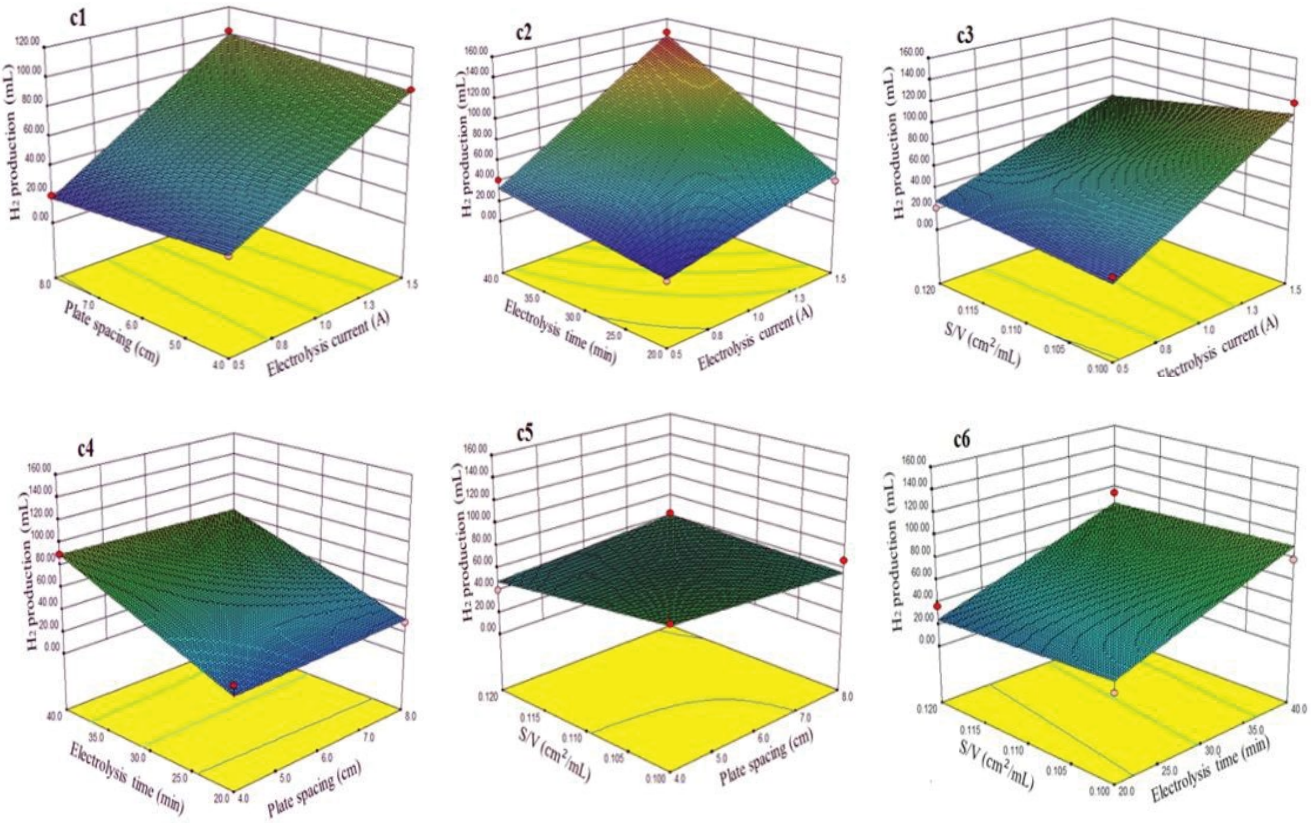

Fig. 12. Effects of electrolysis current, plate spacing, electrolysis time, and *S*/*V* on H_2 production.

lower than that with minimum H_2 production. Thus, gas production affects the treatment effect of EC. The relative errors between the measured results and the predicted results are less than 2.5%, and the measured results are in good agreement with the predicted results. This finding indicates that the RSM model is feasible for optimizing the parameters of EC process to control gas production and consider the treatment effect. The actual maximum hydrogen production is 140.38 mL/m^3 (volume fraction of approximately 0.15%), and does not reach the explosion limit from a safety point of view. The lower explosion limit of H_2 is 4% of the bulk volume. The EC process can remove turbidity and velocity of FFF better than other processes, such as flocculation and adsorption. The parameters of EC process explored in this study can ensure safe production and efficient treatment. Therefore, the results of this study can serve as reference on the treatment of actual FFF in oilfield and can ensure the stability of the EC process.

4. Conclusions

This study demonstrates that the RSM model can optimize and predict the maximum/minimum H_2 production process conditions and treatment effect of EC treatment of FFF. Under the maximum H_2 production condition of I = 1.5 A, d = 8.0 cm, t = 40.0 min, and S/V = 0.12 cm^2/mL, the measured turbidity removal rate, decolorization rate, and H_2 production are 85.96%, 87%, and 140.38 mL, respectively. However, under the minimum H_2 production condition of I = 0.5 A, d = 8.0 cm, t = 20.0 min, and S/V = 0.11 cm^2/mL, the measured turbidity removal rate, decolorization rate, and H_2 production are 89.52%, 95.23%, and 7.95 mL, respectively. Under the maximum/minimum H_2 production conditions, the relative error between all the predicted response values and the measured value is less than 2.5% (Table 7). Therefore, the EC treatment effect and H_2 production of the FFF can be feasibly controlled by optimizing the corresponding technological parameters. Accordingly, the RSM can be used to provide scientific reference for the selection of process conditions, the control of electrolysis H_2 production, and the efficient and safe use of EC.

Funding

This research was financially supported by the Key Technologies R&D Program of China (No. 2016ZX05040-003).

Declaration of interests

The authors declare that they have no known competing financial interests or personal relationships that could have appeared to influence the work reported in this paper.

Acknowledgments

We thanked the Sinopec Fuling Shale Gas Field for offering fracturing flow-back fluid data for our work.

References

[1] G. Tai, Y. Qu, Y. Wang, M. Wu, Research and application of on-line detection and control technology for fracturing fluid, Miner. Metall., 28 (2019) 89–93.
[2] A.C. Ground Water Protection Council, Modern Shale Gas Development in the United States: A Primer, United States Department of Energy, Office of Fossil Energy, Washington, D.C., 2009.
[3] K. Wang, T. Li, G. Lv, Research progresses on treatment technologies of oilfield fracturing flow-back fluid, Chem. Eng. Equip., 2 (2019) 246–247.
[4] Y. Liu, W. Chen, S. Zhang, D.P. Shi, M.J. Zhu, Assessment of gas production and electrochemical factors for fracturing flow-back fluid treatment in Guangyuan oilfield, Environ. Eng. Res., 24 (2018) 521–528.
[5] J. Wang, J. Li, K. Lei, X. Zhang, P. Lu, L. Qiang, S. Wei, Research progress in fracturing flow-back fluid treatment technology, Appl. Chem. Ind., 46 (2017) 1414–1416+1423.
[6] Y. Gao, J. Zhao, D. Ji, Two-stage oxidation-coagulation treatment on the recycling of fracturing flow-back fluid, Technol. Water Treat., 41 (2015) 115–118.
[7] J. Du, C. Qu, T. Yu, Adsorption of boron in fracturing flow-back fluid by XSC-700 resin, Chem. Eng. (China), 47 (2019) 29–34.
[8] J. Wu, C. Li, M. Wang, Z. Xiao, Experimental research on the treatment of fracturing flowback fluid by the distillation method, Ind. Water Treat., 37 (2017) 37–41.
[9] H. Niu, B. Jiang, Y. Du, Study on micro-electrolytic treatment of fracturing flow-back fluid in west sichuan oilfield, J. Chongqing Univ. Sci. Technol., Nat. Sci. Ed., 13 (2011) 100–102.
[10] C. Geng, R. Qiao, G. Chen, B. Yu, H. Li, Y. Wang, D. Xu, S. Yang, Y. Tian, The treatment technologies of hydraulic fracturing fluid flowback of shale gas, Energy Environ. Prot., 30 (2016) 12–16+56.
[11] J. Song, Experiment on oxidation treatment of fracturing flowback fluid from a gas field, Environ. Prot. Oil Gas Fields, 29 (2019) 12–15+18+60.
[12] A. Chen, B. Wang, H. Ren, Composite experimental research on fracturing liquid of preoxidation-coagu-flocculation-ozone deeply oxidation process, Sci. Technol. Chem. Ind., 19 (2011) 26–30.
[13] Z. Hu, T. Zhang, Z. Zhu, P. Luo, T. Huang, Research on the treatment of fracturing flow-back fluid by the coagulation-advanced oxidation combined technology, Ind. Water Treat., 38 (2018) 81–84+94.
[14] H. Ren, J. Wang, W. Zhu, T. Yu, Study on scale prevention of shale gas fracturing backflow fluid treated by ceramic membrane, Ind. Water Treat., 40 (2020) 19–22.
[15] S. Wang, X. Zhao, Z. Li, Q. Yu, Research progresses on treatment technologies of oilfield fracturing flow-back fluid, Environ. Prot. Chem. Ind., 36 (2016) 493–499.
[16] M. Dolatabadi, M. Mehrabpour, M. Esfandyari, S. Ahmadzadeh, Adsorption of tetracycline antibiotic onto modified zeolite: experimental investigation and modeling, MethodsX, 7 (2020) 100885, doi: 10.1016/j.mex.2020.100885.
[17] J. Wu, W. Wu, Y. Yan, M. Wang, Z. Xiao, Research on the treatment status and difficulties of fracturing flowback, Technol. Water Treat., 44 (2018) 12–16.
[18] W. Chen, J. Zhang, J. Zhu, G. Tan, F. Meng, B. Jing, R. Li, Research progress in the composite process of advanced treatment of oil field fracturing flow back liquid, Ind. Water Treat., 36 (2016) 10–14.
[19] D. Zhou, X. Shi, B. Li, F. Wang, Oil and gas field acidification and fracturing flow back treatment technology, Petrochem. Ind. Appl., 37 (2018) 97–99.
[20] M. Mousazadeh, Z. Naghdali, Z. Al-Qodah, S.M. Alizadeh, E.K. Niaragh, S. Malekmohammadi, P.V. Nidheesh, E.P. Roberts, M. Sillanpää, M.M. Emamjomeh, A systematic diagnosis of state of the art in the use of electrocoagulation as a sustainable technology for pollutant treatment: an updated review, Sustainable Energy Technol. Assess., 47 (2021) 101353, doi: 10.1016/j.seta.2021.101353.
[21] W. Chen, P. Mei, Electrochemical Technology for Environmental Pollution Control, Petroleum Industry Press, Beijing, 2013.
[22] S. Ahmadzadeh, A. Kassim, M. Rezayi, Y. Abdollahi, G.H. Rounaghi, A conductometric study of complexation reaction between Meso-octamethylcalix[4]pyrrole with titanium cation in acetonitrile–ethanol binary mixtures, Int. J. Electrochem. Sci., 6 (2011) 4749–4759.
[23] S. Ahmadzadeh, M. Rezayi, H. Karimi-Maleh, Y. Alias, Conductometric measurements of complexation study between 4-isopropylcalix[4]arene and Cr^{3+} cation in THF–DMSO binary solvents, Measurement, 70 (2015) 214–224.
[24] J.N. Hakizimana, B. Gourich, M. Chafi, Y. Stiriba, C. Vial, P. Drogui, J. Naja, Electrocoagulation process in water treatment: a review of electrocoagulation modeling approaches, Desalination, 404 (2017) 1–21.
[25] M. Dolatabadi, T. Świergosz,S. Ahmadzadeh, Electro-Fenton approach in oxidative degradation of dimethyl phthalate – the treatment of aqueous leachate from landfills, Sci. Total Environ., 772 (2021) 145323, doi: 10.1016/j.scitotenv.2021.145323.
[26] T. Karchiyappan, A review on hydrogen energy production from electrochemical system: benefits and challenges, Energy Sources, Part A, 41 (2019) 902–909.
[27] O. Sahu, B. Mazumdar, P.K. Chaudhari, Treatment of wastewater by electrocoagulation: a review, Environ. Sci. Pollut. Res., 21 (2014) 2397–2413.
[28] S. Ahmadzadeh, F. Karimi, N. Atar, E.R. Sartori, E. Faghih-Mirzaei, E. Afsharmanesh, Synthesis of CdO nanoparticles

using direct chemical precipitation method: fabrication of novel voltammetric sensor for square wave voltammetry determination of chlorpromazine in pharmaceutical samples, Inorg. Nano-Metal Chem., 47 (2017) 347–353.
[29] R. Mores, H. Treichel, C.A. Zakrzevski, A. Kunz, J. Steffens, R.M. Dallago, Remove of phosphorous and turbidity of swine wastewater using electrocoagulation under continuous flow, Sep. Purif. Technol., 171 (2016) 112–117.
[30] M. Shen, Y. Zhang, E. Almatrafi, T. Hu, C. Zhou, B. Song, Z. Zeng, G. Zeng, Efficient removal of microplastics from wastewater by an electrocoagulation process, Chem. Eng. J., 428 (2022) 131161, doi: 10.1016/j.cej.2021.131161.
[31] M. Mousazadeh, S.M. Alizadeh, Z. Frontistis, I. Kabdaşlı, E. Karamati Niaragh, Z. Al Qodah, Z. Naghdali, A.E.D. Mahmoud, M.A. Sandoval, E. Butler, M. Mahdi Emamjomeh, Electrocoagulation as a promising defluoridation technology from water: a review of state of the art of removal mechanisms and performance trends, Water, 13 (2021) 656, doi: 10.3390/w13050656.
[32] J.-W. Feng, Y.-B. Sun, Z. Zheng, J.-B. Zhang, L.I. Shu, Y.-C. Tian, Treatment of tannery wastewater by electrocoagulation, J. Environ. Sci. (China), 19 (2007) 1409–1415.
[33] F.L. Lobo, H. Wang, T. Huggins, J. Rosenblum, K.G. Linden, Z.J. Ren, Low-energy hydraulic fracturing wastewater treatment via AC powered electrocoagulation with biochar, J. Hazard. Mater., 309 (2016) 180–184.
[34] Y. Li, T. Zhang, Y. Li, W. Tang, Treatment of fracturing flow-back fluid by electrochemistry technology and reconfiguration of polymer fracturing fluid, Mod. Chem. Ind., 39 (2019) 186–190.
[35] Y. Wang, Q. Li, S. Huang, Y. Wan, Y. Qu, M. Wu, Development and application of electrochemical treatment device for fracturing flowback fluid, Mod. Chem. Ind., 38 (2018) 171–174.
[36] Y. Zhang, X. Cui, S. Liu, W. Zhu, X. Han, Y. Wang, Treatment of oil field fracturing flowback wastewater based on 3D/O_3 process, China Environ. Sci., 40 (2020) 2270–2275.
[37] Y. Xu, Y. Jin, L. Chen, H. Liu, M. Zhang, Pilot test study on treatment of fracturing fluid by three-dimensional electrocatalytic oxidation process, Nat. Gas Oil., 38 (2020) 100–104.
[38] Y. Wang, X. Wu, J. Yi, J. Dai, New three-dimensional electrochemical oxidation system for treatment of fracturing flow-back fluid, Environ. Prot. Chem. Ind., 38 (2018) 251–255.
[39] K.A. Sitterley, J. Rosenblum, B. Ruyle, R. Keliher, K.G. Linden, Factors impacting electrocoagulation treatment of hydraulic fracturing fluids and removal of common fluid additives and scaling ions, J. Environ. Chem. Eng., 8 (2020) 103728, doi: 10.1016/j.jece.2020.103728.
[40] Y. Liu, W. Chen, D. Wu, Advances on the effect and harm of gas generation in electrochemical treatment process of wastewater, Appl. Chem. Ind., 47 (2018) 2235–2241.
[41] GB/T 6920-1986, Water Quality–Determination of pH Value–Glass Electrode Method, Standards Press of China, Beijing, 1987.
[42] Z. Fanliang, L. Xiantao, Determination of the colority of water samples by spectrophotometry, 2006, pp. 69–72+77.
[43] HJ 501-2009, Water Quality–Determination of Total Organic Carbon-Combustion Oxidation Nondispersive Infrared Absorption Method, Standards Press of China, Beijing, 2009.
[44] N. Gros, M.F. Camões, C. Oliveira, M. Silva, Ionic composition of seawaters and derived saline solutions determined by ion chromatography and its relation to other water quality parameters, J. Chromatogr. A, 1210 (2008) 92–98.
[45] HJ 637-2018, Water Quality–Determination of Petroleum, Animal Fats and Vegetable Oils–Infrared Spectrophotometry, Standards Press of China, Beijing, 2018.
[46] HJ 828-2017, Water Quality–Determination of the Chemical Oxygen Demand–Dichromate Method, Standards Press of China, Beijing, 2017.
[47] HJ1075-2019, Water Quality–Determination of Turbidity–Nephelometry, Standards Press of China, Beijing, 2020.
[48] M.M. Emamjomeh, H.A. Jamali, Z. Naghdali, M. Mousazadeh, Carwash wastewater treatment by the application of an environmentally friendly hybrid system: an experimental design approach, Desal. Water Treat., 160 (2019) 171–177.
[49] M. Dolatabadi, M.T. Ghaneian, C. Wang, S. Ahmadzadeh, Electro-Fenton approach for highly efficient degradation of the herbicide 2,4-dichlorophenoxyacetic acid from agricultural wastewater: process optimization, kinetic and mechanism, J. Mol. Liq., 334 (2021) 116116, doi: 10.1016/j.molliq.2021.116116.
[50] T. Ntambwe Kambuyi, F. Eddaqaq, A. Driouich, B. Bejjany, B. Lekhlif, H. Mellouk, K. Digua, A. Dani, Using response surface methodology (RSM) for optimizing turbidity removal by electrocoagulation/electro-flotation in an internal loop airlift reactor, Water Supply, 19 (2019) 2476–2484.
[51] V. Preethi, S.T. Ramesh, R. Gandhimathi, P.V. Nidheesh, Optimization of batch electrocoagulation process using Box–Behnken experimental design for the treatment of crude vegetable oil refinery wastewater, J. Dispersion Sci. Technol., 41 (2019) 592–599.
[52] M. Behbahani, M.M. Alavi, M. Arami, A comparison between aluminum and iron electrodes on removal of phosphate from aqueous solutions by electrocoagulation process, Int. J. Environ. Res., 5 (2011) 403–412.
[53] D. Sharma, P.K. Chaudhari, A.K. Prajapati, Removal of chromium(VI) and lead from electroplating effluent using electrocoagulation, Sep. Sci. Technol., 55 (2020) 321–331.
[54] S. Badakhshan, S. Ahmadzadeh, A. Mohseni-Bandpei, M. Aghasi, A. Basiri, Potentiometric sensor for iron(III) quantitative determination: experimental and computational approaches, BMC Chem., 13 (2019) 1–12.
[55] M. Fouladgar, S. Ahmadzadeh, Application of a nanostructured sensor based on NiO nanoparticles modified carbon paste electrode for determination of methyldopa in the presence of folic acid, Appl. Surf. Sci., 379 (2016) 150–155.
[56] R. Mohtashami, J.Q. Shang, Electroflotation for treatment of industrial wastewaters: a focused review, Environ. Process., 6 (2019) 325–353.
[57] C. Ding, H. Zeng, Y. Huang, F. Peng, Z. Xu, Study on the decolorizaton of simulated azo dye wastewater with electro coagulation method, Text. Aux., 29 (2012) 39–41.
[58] G. Zhang, S. Gong, F. Wu, S. Yang, L. Liu, Study on optimum parameter for turbidity removal in rainwater collection by electro-coagulation in northwest region, J. Water Resour. Water Eng., 23 (2012) 38–41.
[59] I. Zongo, J. Leclerc, H.A. Maiga, J. Wéthé, F. Lapicque, Removal of hexavalent chromium from industrial wastewater by electrocoagulation: a comprehensive comparison of aluminium and iron electrodes, Sep. Purif. Technol., 66 (2009) 159–166.
[60] A. Sarpola, V. Hietapelto, J. Jalonen, J. Jokela, R.S. Laitinen, Identification of the hydrolysis products of $AlCl_3 \cdot 6H_2O$ by electrospray ionization mass spectrometry, J. Mass Spectrom., 39 (2004) 423–430.
[61] M. Rezayi, L.Y. Heng, A. Kassim, S. Ahmadzadeh, Y. Abdollahi, H. Jahangirian, Immobilization of tris(2 pyridyl) methylamine in a PVC-membrane sensor and characterization of the membrane properties, Chem. Cent. J., 6 (2012) 1–6.
[62] D. Li, C. Wang, X. He, R. Wang, N. Zhao, L. Huang, Y. Qian, Removal of ammonia from micro-polluted water by electrochemical oxidation process, Chin. J. Environ. Eng., 6 (2012) 1553–1558.
[63] S.D. Ashrafi, G.H. Safari, K. Sharafi, H. Kamani, J. Jaafari, Adsorption of 4-nitrophenol on calcium alginate-multiwall carbon nanotube beads: modeling, kinetics, equilibriums and reusability studies, Int. J. Biol. Macromol., 185 (2021) 66–76.
[64] J. Jaafaria, K. Yaghmaeiana, Response surface methodological approach for optimizing heavy metal biosorption by the blue-green alga *Chroococcus disperses*, Desal. Water Treat., 142 (2019) 225–234.